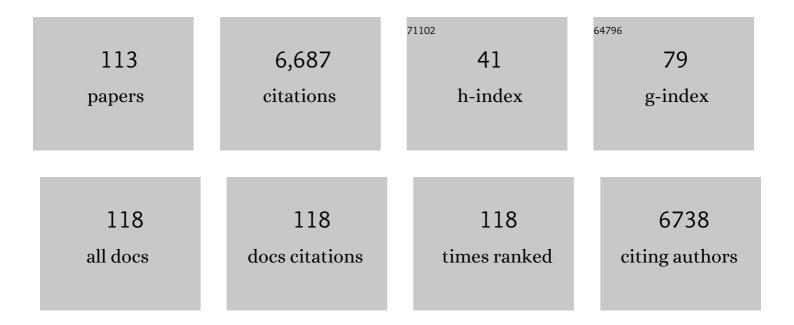
List of Publications by Year in descending order

Source: https://exaly.com/author-pdf/5398542/publications.pdf Version: 2024-02-01



YE-FENC YAO

#	Article	IF	CITATIONS
1	Electrosorption behavior of graphene in NaCl solutions. Journal of Materials Chemistry, 2009, 19, 6773.	6.7	352
2	Heterogeneity in polymer melts from melting of polymer crystals. Nature Materials, 2005, 4, 635-641.	27.5	321
3	Review on carbon-based composite materials for capacitive deionization. RSC Advances, 2015, 5, 15205-15225.	3.6	319
4	Tunable and Switchable Dielectric Constant in an Amphidynamic Crystal. Journal of the American Chemical Society, 2013, 135, 5230-5233.	13.7	307
5	Electrospun carbon nanofibers as anode materials for sodium ion batteries with excellent cycle performance. Journal of Materials Chemistry A, 2014, 2, 4117.	10.3	272
6	Covalent-organic-frameworks derived N-doped porous carbon materials as anode for superior long-life cycling lithium and sodium ion batteries. Carbon, 2017, 116, 686-694.	10.3	260
7	Nanoarchitectured metal–organic framework/polypyrrole hybrids for brackish water desalination using capacitive deionization. Materials Horizons, 2019, 6, 1433-1437.	12.2	241
8	A flexible, high-voltage and safe zwitterionic natural polymer hydrogel electrolyte for high-energy-density zinc-ion hybrid supercapacitor. Chemical Engineering Journal, 2020, 392, 123733.	12.7	212
9	ZnS nanoparticles decorated on nitrogen-doped porous carbon polyhedra: a promising anode material for lithium-ion and sodium-ion batteries. Journal of Materials Chemistry A, 2017, 5, 20428-20438.	10.3	192
10	Metal-organic frameworks derived yolk-shell ZnO/NiO microspheres as high-performance anode materials for lithium-ion batteries. Chemical Engineering Journal, 2018, 335, 579-589.	12.7	191
11	Design of pomegranate-like clusters with NiS <sub>2</sub> nanoparticles anchored on nitrogen-doped porous carbon for improved sodium ion storage performance. Journal of Materials Chemistry A, 2018, 6, 6595-6605.	10.3	159
12	Rational design of MoS2-reduced graphene oxide sponges as free-standing anodes for sodium-ion batteries. Chemical Engineering Journal, 2018, 332, 260-266.	12.7	159
13	Extraordinary capacitive deionization performance of highly-ordered mesoporous carbon nano-polyhedra for brackish water desalination. Environmental Science: Nano, 2019, 6, 981-989.	4.3	150
14	Ti3C2 MXenes-derived NaTi2(PO4)3/MXene nanohybrid for fast and efficient hybrid capacitive deionization performance. Chemical Engineering Journal, 2021, 407, 127148.	12.7	140
15	Organic enantiomeric high- <i>T</i> <sub>c</sub> ferroelectrics. Proceedings of the National Academy of Sciences of the United States of America, 2019, 116, 5878-5885.	7.1	137
16	In-situ encapsulation of Ni3S2 nanoparticles into N-doped interconnected carbon networks for efficient lithium storage. Chemical Engineering Journal, 2019, 378, 122108.	12.7	136
17	Dynamics of a caged imidazolium cation–toward understanding the order-disorder phase transition and the switchable dielectric constant. Chemical Communications, 2015, 51, 4568-4571.	4.1	121
18	Metal–organic framework-engaged formation of a hierarchical hybrid with carbon nanotube inserted porous carbon polyhedra for highly efficient capacitive deionization. Journal of Materials Chemistry A, 2016, 4, 5467-5473.	10.3	117

#	Article	IF	CITATIONS
19	Metal–organic-frameworks-derived NaTi <sub>2</sub> (PO <sub>4</sub> ) <sub>3</sub> /carbon composites for efficient hybrid capacitive deionization. Journal of Materials Chemistry A, 2019, 7, 12126-12133.	10.3	115
20	Surface hydrogen bonding can enhance photocatalytic H2 evolution efficiency. Journal of Materials Chemistry A, 2013, 1, 14089.	10.3	113
21	Synergistic coupling of NiS1.03 nanoparticle with S-doped reduced graphene oxide for enhanced lithium and sodium storage. Chemical Engineering Journal, 2021, 407, 127199.	12.7	110
22	Facile self-templating synthesis of layered carbon with N, S dual doping for highly efficient sodium storage. Carbon, 2021, 173, 31-40.	10.3	107
23	In-situ construction of g-C3N4/Mo2CTx hybrid for superior lithium storage with significantly improved Coulombic efficiency and cycling stability. Chemical Engineering Journal, 2021, 410, 128349.	12.7	105
24	A Chemically Triggered and Thermally Switched Dielectric Constant Transition in a Metal Cyanide Based Crystal. Angewandte Chemie - International Edition, 2015, 54, 6206-6210.	13.8	103
25	Transferring Lithium Ions in Nanochannels: A PEO/Li <sup>+</sup> Solid Polymer Electrolyte Design. Angewandte Chemie - International Edition, 2014, 53, 3631-3635.	13.8	102
26	Geometric isotope effect of deuteration in a hydrogen-bonded host–guest crystal. Nature Communications, 2018, 9, 481.	12.8	76
27	Facile dual doping strategy <i>via</i> carbonization of covalent organic frameworks to prepare hierarchically porous carbon spheres for membrane capacitive deionization. Chemical Communications, 2018, 54, 14009-14012.	4.1	74
28	Metal-organic frameworks converted flower-like hybrid with Co3O4 nanoparticles decorated on nitrogen-doped carbon sheets for boosted lithium storage performance. Chemical Engineering Journal, 2018, 354, 172-181.	12.7	68
29	Insights into the storage mechanism of 3D nanoflower-like V3S4 anode in sodium-ion batteries. Chemical Engineering Journal, 2022, 427, 130936.	12.7	67
30	Heterogeneous Distribution of Entanglements in a Nonequilibrium Polymer Melt of UHMWPE: Influence on Crystallization without and with Graphene Oxide. Macromolecules, 2016, 49, 7497-7509.	4.8	64
31	Recent progress on metal–organic framework-derived materials for sodium-ion battery anodes. Inorganic Chemistry Frontiers, 2020, 7, 567-582.	6.0	63
32	Heterogeneous ice nucleation correlates with bulk-like interfacial water. Science Advances, 2019, 5, eaat9825.	10.3	60
33	Synergistic Promotion of Single-Atom Co Surrounding a PtCo Alloy Based On a g-C <sub>3</sub> N <sub>4</sub> Nanosheet for Overall Water Splitting. ACS Catalysis, 2022, 12, 6958-6967.	11.2	59
34	Accurate and Real-Time Temperature Monitoring during MR Imaging Guided PTT. Nano Letters, 2020, 20, 2522-2529.	9.1	56
35	Highly efficient and stable desalination via novel hybrid capacitive deionization with redox-active polyimide cathode. Desalination, 2019, 469, 114098.	8.2	53
36	NMR Study on the Effects of Sodium <i>n</i> -Dodecyl Sulfate on the Coil-to-Globule Transition of Poly( <i>N</i> -isopropylacrylamide) in Aqueous Solutions. Macromolecules, 2011, 44, 6227-6231.	4.8	51

#	Article	IF	CITATIONS
37	Controlling Polymer Architecture through Host-Guest Interactions. Angewandte Chemie - International Edition, 2006, 45, 87-90.	13.8	50
38	Operando NMR spectroscopic analysis of proton transfer in heterogeneous photocatalytic reactions. Nature Communications, 2016, 7, 11918.	12.8	49
39	Prussian blue analogue derived cobalt–nickel phosphide/carbon nanotube composite as electrocatalyst for efficient and stable hydrogen evolution reaction in wide-pH environment. Journal of Colloid and Interface Science, 2022, 616, 210-220.	9.4	49
40	Cocoon derived nitrogen enriched activated carbon fiber networks for capacitive deionization. Journal of Electroanalytical Chemistry, 2017, 804, 179-184.	3.8	47
41	The construction of a two-dimensional organic–inorganic hybrid double perovskite ferroelastic with a high <i>T</i> <sub>c</sub> and narrow band gap. Chemical Science, 2022, 13, 4794-4800.	7.4	46
42	Switching Dielectric Constant Near Room Temperature in a Molecular Crystal. Advanced Science, 2015, 2, 1500029.	11.2	42
43	An above-room-temperature phosphonium-based molecular ferroelectric perovskite, [(CH3)4P]CdCl3, with Sb3+-doped luminescence. NPG Asia Materials, 2019, 11, .	7.9	42
44	Metal chelate induced <i>in situ</i> wrapping of Ni <sub>3</sub> S <sub>2</sub> nanoparticles into N, S-codoped carbon networks for highly efficient sodium storage. Inorganic Chemistry Frontiers, 2019, 6, 694-704.	6.0	40
45	Novel hybrid capacitive deionization constructed by a redox-active covalent organic framework and its derived porous carbon for highly efficient desalination. Journal of Materials Chemistry A, 2019, 7, 25305-25313.	10.3	40
46	N-doped carbon@Cu core–shell nanostructure with nearly full solar spectrum absorption and enhanced solar evaporation efficiency. Journal of Materials Chemistry A, 2022, 10, 9575-9581.	10.3	37
47	BrÃ,nsted base site engineering of graphitic carbon nitride for enhanced photocatalytic activity. Journal of Materials Chemistry A, 2017, 5, 19227-19236.	10.3	36
48	Identifying Catalytically Active Mononuclear Peroxoniobate Anion of Ionic Liquids in the Epoxidation of Olefins. ACS Catalysis, 2018, 8, 4645-4659.	11.2	36
49	Highly Efficient Epoxidation of Allylic Alcohols with Hydrogen Peroxide Catalyzed by Peroxoniobate-Based Ionic Liquids. ACS Catalysis, 2016, 6, 3354-3364.	11.2	35
50	Novel membrane-free hybrid capacitive deionization with a radical polymer anode for stable desalination. Desalination, 2020, 481, 114379.	8.2	34
51	Surface Passivation and Energetic Modification Suppress Nonradiative Recombination in Perovskite Solar Cells. Nano-Micro Letters, 2022, 14, 108.	27.0	34
52	<sup>13</sup> C Solid State NMR Characterization of Structure and Orientation Development in the Narrow and Broad Molar Mass Disentangled UHMWPE. Macromolecules, 2014, 47, 1371-1382.	4.8	33
53	Phase Structure and Helical Jump Motion of Poly(ethylene oxide)/LiCF <sub>3</sub> SO <sub>3</sub> Crystalline Complex: A High-Resolution Solid-State <sup>13</sup> C NMR Approach. Macromolecules, 2013, 46, 4447-4453.	4.8	30
54	Viologen-bridged polyaniline based multifunctional heterofilms for all-solid-state supercapacitors and memory devices. European Polymer Journal, 2018, 98, 125-136.	5.4	29

#	Article	IF	CITATIONS
55	Origin of Photocatalytic Activity in Ti <sup>4+</sup> /Ti <sup>3+</sup> Core–Shell Titanium Oxide Nanocrystals. Journal of Physical Chemistry C, 2019, 123, 20949-20959.	3.1	29
56	Light-conversion phosphor nanoarchitectonics for improved light harvesting in sensitized solar cells. Journal of Photochemistry and Photobiology C: Photochemistry Reviews, 2021, 47, 100404.	11.6	29
57	Self-Healing Amorphous Polymers with Room-Temperature Phosphorescence Enabled by Boron-Based Dative Bonds. ACS Applied Polymer Materials, 2020, 2, 699-705.	4.4	27
58	Segmental Dynamics of PEO/LiClO <sub>4</sub> Complex Crystals and Their Influence on the Li <sup>+</sup> â€Ion Transportation in Crystal Lattices: A <sup>13</sup> C Solidâ€State NMR Approach. Chemistry - A European Journal, 2011, 17, 8941-8946.	3.3	25
59	Facile self-assembly of carbon-free vanadium sulfide nanosheet for stable and high-rate lithium-ion storage. Journal of Colloid and Interface Science, 2022, 607, 145-152.	9.4	25
60	Suppressing the oxygen-related parasitic reactions in NaTi2(PO4)3-based hybrid capacitive deionization with cation exchange membrane. Journal of Colloid and Interface Science, 2021, 591, 139-147.	9.4	24
61	Boosting the lithium storage performance by synergistically coupling ultrafine heazlewoodite nanoparticle with N, S co-doped carbon. Journal of Colloid and Interface Science, 2021, 604, 368-377.	9.4	24
62	Revealing structure and dynamics in host–guest supramolecular crystalline polymer electrolytes by solid-state NMR: Applications to β-CD-polyether/Li+ crystal. Polymer, 2016, 105, 310-317.	3.8	23
63	In-situ fabrication of few-layered MoS2 wrapped on TiO2-decorated MXene as anode material for durable lithium-ion storage. Journal of Colloid and Interface Science, 2021, 604, 30-38.	9.4	23
64	A ferroelastic molecular rotor crystal showing inverse temperature symmetry breaking. Inorganic Chemistry Frontiers, 2021, 8, 2809-2816.	6.0	22
65	Crosslinking Nanoarchitectonics of Nitrogenâ€doped Carbon/MoS <sub>2</sub> Nanosheets/Ti <sub>3</sub> C <sub>2</sub> T <sub><i>x</i></sub> MXene Hybrids for Highly Reversible Sodium Storage. ChemSusChem, 2021, 14, 5293-5303.	6.8	22
66	Fast Lithiumâ€lon Transportation in Crystalline Polymer Electrolytes. ChemPhysChem, 2018, 19, 45-50.	2.1	21
67	Ionic Liquid Stabilized Niobium Oxoclusters Catalyzing Oxidation of Sulfides with Exceptional Activity. Chemistry - A European Journal, 2019, 25, 4206-4217.	3.3	20
68	Facile in-situ synthesis of heazlewoodite on nitrogen-doped reduced graphene oxide for enhanced sodium storage. Journal of Colloid and Interface Science, 2021, 594, 35-46.	9.4	20
69	NMR Study of Thermoresponsive Hyperbranched Polymer in Aqueous Solution with Implication on the Phase Transition. Macromolecules, 2013, 46, 9688-9697.	4.8	17
70	Viologen-based conjugated ionic polymer for nonvolatile rewritable memory device. European Polymer Journal, 2017, 94, 222-229.	5.4	16
71	Polyaniline coated MOF-derived Mn2O3 nanorods for efficient hybrid capacitive deionization. Environmental Research, 2022, 212, 113331.	7.5	16
72	Probing the Fast Lithium-Ion Transport in Small-Molecule Solid Polymer Electrolytes by Solid-State NMR. Macromolecules, 2020, 53, 10078-10085.	4.8	15

YE-FENG YAO

#	Article	IF	CITATIONS
73	lonic Conductivity of β yclodextrin–Polyethyleneâ€Oxide/Alkaliâ€Metalâ€Salt Complex. Chemistry - A European Journal, 2015, 21, 6346-6349.	3.3	14
74	Selective hydrogen–deuterium exchange in graphitic carbon nitrides: probing the active sites for photocatalytic water splitting by solid-state NMR. Journal of Materials Chemistry A, 2021, 9, 3985-3994.	10.3	14
75	Shape and size effects on photocatalytic hydrogen production <i>via</i> Pd/C <sub>3</sub> N <sub>4</sub> photocatalysts under visible light. Catalysis Science and Technology, 2020, 10, 5438-5442.	4.1	13
76	Formamidinium lead triiodide perovskites with improved structural stabilities and photovoltaic properties obtained by ultratrace dimethylamine substitution. NPG Asia Materials, 2022, 14, .	7.9	13
77	In situ NMR Investigation of the Photoresponse of Perovskite Crystal. Matter, 2020, 3, 2042-2054.	10.0	12
78	Metastable alloying structures in MAPbI3â^'xClx crystals. NPG Asia Materials, 2020, 12, .	7.9	12
79	Cooperative Motion in Water–Methanol Clusters Controls the Reaction Rates of Heterogeneous Photocatalytic Reactions. Journal of the American Chemical Society, 2021, 143, 10940-10947.	13.7	12
80	NMR Study on the Roles of Li <sup>+</sup> in the Cellulose Dissolution Process. ACS Sustainable Chemistry and Engineering, 2019, 7, 618-624.	6.7	11
81	Solvent Water Controls Photocatalytic Methanol Reforming. Journal of Physical Chemistry Letters, 2020, 11, 3738-3744.	4.6	11
82	Cu-based MOF-derived architecture with Cu/Cu2O nanospheres anchored on porous carbon nanosheets for efficient capacitive deionization. Environmental Research, 2022, 210, 112909.	7.5	11
83	Rapid Identification of Adulteration in Edible Vegetable Oils Based on Low-Field Nuclear Magnetic Resonance Relaxation Fingerprints. Foods, 2021, 10, 3068.	4.3	11
84	Well-dispersed ZIF-derived N-doped carbon nanoframes with anchored Ru nanoclusters as HER electrocatalysts. International Journal of Hydrogen Energy, 2022, 47, 14836-14846.	7.1	11
85	Interfacial water in mesopores and its implications to the surface features – A solid state NMR study. Applied Surface Science, 2019, 484, 1154-1160.	6.1	10
86	Thermoresponsive Hyperbranched Polymers with Spatially Isomerized Groups: NMR Implication to Their Thermoresponsive Behaviors. Macromolecules, 2017, 50, 9647-9655.	4.8	10
87	lonic liquid-stabilized vanadium oxo-clusters catalyzing alkane oxidation by regulating oligovanadates. Catalysis Science and Technology, 2020, 10, 7601-7612.	4.1	9
88	Probing the methanol heterogeneous photochemistry processes by operando NMR – The role of bulk water. Journal of Catalysis, 2019, 378, 36-41.	6.2	8
89	Enhanced photocatalytic reduction of Cr(vi) to Cr(iii) over g-C3N4 catalysts with Ag nanoclusters in conjunction with Cr(iii) quantification based on operando low-field NMR relaxometry. Environmental Science: Nano, 2020, 7, 2823-2832.	4.3	8
90	Solid-state NMR study of adsorbed water molecules in covalent organic framework materials. Microporous and Mesoporous Materials, 2020, 305, 110287.	4.4	8

#	Article	IF	CITATIONS
91	Role of Organic Fluoride Salts in Stabilizing Niobium Oxo-Clusters Catalyzing Epoxidation. Langmuir, 2021, 37, 8190-8203.	3.5	8
92	Self-Enhanced Acoustic Impedance Difference Strategy for Detecting the Acidic Tumor Microenvironment. ACS Nano, 2022, 16, 4217-4227.	14.6	8
93	Unexpected Role of Short Chains in Entangled Polymer Networks. ACS Macro Letters, 2022, 11, 669-674.	4.8	8
94	Operando NMR study on the effect of photon flux and wavelength on photocatalytic reforming of methanol. Journal of Catalysis, 2020, 382, 173-180.	6.2	7
95	Probing the Dynamics of Li+ Ions on the Crystal Surface: A Solid-State NMR Study. Polymers, 2020, 12, 391.	4.5	6
96	Preparation of the individual compact single-chain globular particulates of Poly(N-isopropylacrylamide). Colloid and Polymer Science, 2006, 284, 935-940.	2.1	5
97	Annealing To Induce Formation of Defects in Polyether/Li <sup>+</sup> Complex Crystals – A Way To Significantly Enhance the Crystalline Segmental Mobility. Macromolecules, 2019, 52, 5971-5976.	4.8	5
98	Solvent-polymer guest exchange in a carbamazepine inclusion complex: structure, kinetics and implication for guest selection. CrystEngComm, 2019, 21, 2164-2173.	2.6	5
99	Specific thermoresponsive behaviours exhibited by optically active and inactive phenylalanine modified hyperbranched polyethylenimines in water. Chinese Journal of Polymer Science (English Edition), 2017, 35, 1035-1042.	3.8	4
100	Dynamic heterogeneity in homogeneous polymer melts. Soft Matter, 2021, 17, 6081-6087.	2.7	4
101	A Novel Salenâ€based Porous Framework Polymer as Durable Anode for Lithiumâ€ŀon Storage. ChemSusChem, 2021, 14, 4601-4608.	6.8	4
102	A Small Lattice Change Induces Significant Dynamic Changes of CH3NH3+ Caged in Hybrid Perovskite Crystals: Toward Understanding the Interplay between Host Lattices and Guest Molecules. Inorganic Chemistry, 2019, 58, 7426-7432.	4.0	3
103	Illumination-Induced Changes in Methylammonium Lead Bromine Perovskites. An In Situ 2H NMR Study. Journal of Physical Chemistry C, 2021, 125, 9908-9915.	3.1	3
104	Olefin epoxidation with ionic liquid catalysts formed by supramolecular interactions. Molecular Catalysis, 2021, 500, 111342.	2.0	3
105	Tetranuclear ruthenium clusters anchored on polyoxometalates catalyze the hydrogenation of methyl levulinate in water. New Journal of Chemistry, 2021, 45, 21215-21224.	2.8	3
106	Monitoring Cr(VI) photoreduction at different depths by operando low-field NMR relaxometry. Magnetic Resonance Letters, 2022, 2, 170-176.	1.3	3
107	Enhanced hydrogen evolution reaction activity of FeM (MÂ=ÂPt, Pd, Ru, Rh) nanoparticles with N-doped carbon coatings over a wide-pH environment. Molecular Catalysis, 2021, 514, 111830.	2.0	2
108	A-Site Mixing to Adjust the Photovoltaic Performance of a Double-Cation Perovskite: It Is Not Always the Simple Way. Journal of Physical Chemistry Letters, 2021, 12, 11206-11213.	4.6	2

#	Article	IF	CITATIONS
109	Multiple-targeting NMR signal selection by optimal control of nuclear spin singlet. Journal of Magnetic Resonance, 2022, 338, 107188.	2.1	2
110	Operando NMR Spectroscopic Analysis of the Effects of Pt Nanoparticle Size and Crystal Facet Structure on the Alcohol Reforming Reactions. Journal of Physical Chemistry C, 0, , .	3.1	1
111	Colorless Chemical Substance Detection in the Degradation of Tetracycline Based on Operando 1H Nuclear Magnetic Resonance Spectroscopy. Journal of Physical Chemistry C, 2021, 125, 23169-23177.	3.1	Ο
112	Solid-state NMR studies on crystalline solid polymer electrolytes and important cathode materials for lithium-ion batteries. Annual Reports on NMR Spectroscopy, 2020, , 265-308.	1.5	0
113	Evidencing active-site transfer in the hetero-structure photo-catalytic processes via NMR molecular probes. Journal of Catalysis, 2022, , .	6.2	0